Thermal Stability Evaluation of PA6/LLDPE/SEBS-g-DEM Blends

Luis Cataño,[1] *Carmen Albano,**[1,2] *Arquímedes Karam,*[1] *Rosestela Perera,*[3] *Pedro Silva*[4]

Summary: The thermal stability of a polyamide-6/low linear density polyethylene blend (PA6/LLDPE) was studied using thermal analysis techniques. The thermogravimetric studies carried out showed that when a diethyl maleate grafted styrene-ethylene/butadiene-styrene terpolymer (SEBS-g-DEM) is added to the PA6/LLDPE blend there is an actual enhancement of the thermal stability due to the increase in the interfacial area within the blend. The Invariant Kinetic Parameter method (IKP) proved to be a qualitative technique unfolding the type of degradation mechanisms taking place in the material vicinity. Nucleation and phase boundary reactions are the kinetic models of thermal decomposition with the most significant probability of occurring.

Keywords: activation energy; compatibility; IKP; polyethylene (PE)

Introduction

Linear low-density polyethylene (LLDPE) has a widespread range of applications due to its properties arising from the comonomer addition.[1,2,3] From toy design to complex engineering applications, this polymer shows an exceptional performance. However, some of its properties limit its expansion towards new application fields, such as those requiring adhesion characteristics. Hence, there has been recent works related to the modification of the properties of LLDPE involving addition of different polymeric components.

On the other hand, PA6 is one of the engineering plastics most used on industrial applications. It has been blended with LLDPE in order to get the best of both polymers' characteristics in one material. However, because of their different natures, the PA6/LLDPE interface must be optimally increased by means of an interfacial or compatibilizing agent, such as a SEBS terpolymer.[4]

In the present work, the thermal stability of a PA6/LLDPE blend when SEBS-g-DEM is used as a compatibilizer agent was studied.

Experimental Part

Materials

A LLDPE with 1-butene as comonomer (SCLAIR® 11D1) provided by Dupont, a PA6 (Sniamid® ADS 50), a SEBS terpolymer (Kraton®), DEM supplied by Sigma Chemical, dicumyl peroxide provided by Aldrich Chemical, Irganox B1171 and Irganox 1098 supplied by CIBA, were used.

Blend Preparation

The SEBS terpolymer was functionalized through reactive extrusion in a Berstorff ECS-2E25 corotating twin-screw extruder, using DEM as a comonomer and DCP as

[1] Laboratorio de Polímeros, Centro de Química, Instituto Venezolano de Investigaciones Científicas, Km. 11 Carretera Panamericana, Altos de Pipe, Venezuela E-mail: calbano@ivic.ve
[2] Universidad Central de Venezuela, Facultad de Ingeniería, Escuela de Ingeniería Química, Los Chaguaramos, Caracas, Venezuela
[3] Departamento de Mecánica, Universidad Simón Bolívar, Valle de Sartenejas, Caracas, Venezuela
[4] Laboratorio de Física de la Materia Condensada, Centro de Física, Instituto Venezolano de Investigaciones Científicas

Table 1.
Conditions used in blending and SEBS grafting.

Condition	Grafting	Mixing
Temperature profile (°C)	238-227-238-238-238	130-225-238-218-216
Melt Temperature (°C)	244	232
Die Temperature (°C)	225	225
Pressure drop (psi)	1000	750
Screw rate (rpm)	50	110

initiator under the conditions shown in Table 1. The grafting degree achieved in SEBS-g-DEM functionalization lies around 0.4 wt %. This grafting degree was determined according to Rosales et al.[5] by FTIR and a calibration curve.

The PA6/LLDPE (20/80% wt., respectively) and PA6/LLDPE/SEBS-g-DEM blends were prepared in a Werner & Pfleiderer ZSK-30 corotating twin-screw extruder under the conditions shown in Table 1. The compatibilizer (SEBS-g-DEM) was added at a concentration of 5% wt. Irganox B-1171 and Irganox 1098 were added before melt blending (0.5 and 0.25% wt., respectively) to avoid thermal degradation during processing.

Thermogravimetric Analysis (TGA)

Thermograms were obtained by thermogravimetric analysis on a Mettler-Toledo TGA/STDA851^e thermal analyzer under the following conditions: samples of 10 mg each were heated up to a temperature of 800 K under nitrogen atmosphere and various heating rates ($\beta_i = 5$, 15 and 20 °C/min).

Subsequently, thermal kinetic parameters were determined by means of the Invariant Kinetic Parameters method.[6]

Molau Test

The Molau test[7] was performed on the blends in order to determine if there was a possible compatibilizing effect. Samples of the blends were dissolved in concentrated formic acid (2% w/v solution) and allowed to rest for 8 h at room temperature.

Scanning Electron Microscopy

Scanning Electron Microscopy (SEM) analyses were carried out on the cryogenically-fractured surface of compression-molded samples using a Philips 505 microscope. Samples were metallized with gold-palladium.

Invariant Kinetic Parameters (IKP) Method[8,9,10]

To determine the invariant activation energy (E_{inv}) and the pre-exponential factor (A_{inv}) the rate expression, $d\alpha/dt$, was assumed to be equal to the following equation:

$$\frac{d\alpha}{dt} = k \times f(\alpha) \tag{1}$$

where α is the degree of conversion and $k = A \times \exp(-E/RT)$ according to Arrhenius law.

Eighteen apparent activation energies (E_{iv}) and pre-exponential factors (A_{iv}) were determined employing the Coats-Redfern method.[11] The IKP method is based on the principle of the compensation effect quite well reviewed in the literature. For each function $f_j(\alpha)$ proposed by the method, $log(A_j)$ versus E_j is plotted. If a compensation effect is observed, then a linear relationship is seen for each heating rate β_v, which is defined by the following expression:

$$\log A_{iv} = B_v + l_v E_{jv} \tag{2}$$

where A_{iv} and E_{jv} are the apparent pre-exponential factor and the activation energy, respectively, calculated using a function $f_j(\alpha)$ at β_v.

Inappropriate assigning of the kinetic model function results in the distortion of the kinetic parameters and in the false or superficial classification of the compensation effect.

The values B_v and l_v are calculated from the intercept and the slope of the straight lines obtained by Equation (2). Lesnikovich

Table 2.
Degradation functions used in the IKP method.[6]

Kinetic models	$f_j(\alpha)$	$g_j(\alpha)$	Observations
Nucleation and nucleus growth	$\frac{1}{n}(1-\alpha)(-\ln(1-\alpha))^{1-n}$	$(-\ln(1-\alpha))^{n}$	S1-$n=1/4$
			S2-$n=1/3$
			S3-$n=1/2$
			S4-$n=2/3$
Phase boundary reaction	$(1-\alpha)^{n}$	$1-(1-\alpha)$	S6 Plane Symmetry
		$2\left[1-(1-\alpha)^{1/2}\right]$	S7 Cylindrical Symmetry
		$3\left[1-(1-\alpha)^{1/3}\right]$	S8 Spherical Symmetry
Diffusion	$1/2\alpha^{-1}$	α^{2}	S9 Plane Symmetry
	$(-\ln(1-\alpha))^{-1}$	$(1-\alpha)\ln(1-\alpha)+\alpha$	S10 Cylindrical Symmetry
	$3/2\left[(1-\alpha)^{-1/3}-1\right]^{-1}$	$1-2/3\alpha-(1-\alpha)^{2/3}$	S11 Spherical Symmetry
	$3/2(1-\alpha)^{1/3}\left[(1-\alpha)^{-1/3}-1\right]^{-1}$	$\left[(1-\alpha)^{1/3}-1\right]^{2}$	S18 Jander's Type
Potential law	$(1/n)\alpha^{1-n}$	$\alpha^{n}(0<n<2)$	S12-$n=1/4$
			S13-$n=1/3$
			S14-$n=1/2$
			S17-$n=3/2$
Reaction order	$(1-\alpha)$	$-\ln(1-\alpha)$	S5-$n=1$
	$(1/n)(1-\alpha)^{1-n}$	$1-(1-\alpha)^{1/2}$	S15-$n=1/2$
		$1-(1-\alpha)^{1/3}$	S16-$n=1/3$

and Levchik[8,9] discussed the significance of these values and demonstrated the following relationships:

$$B_v = \log(k_v) \tag{3}$$

$$l_v = (2.3RT_v)^{-1} \tag{4}$$

where k_v is the rate constant at of the system at the temperature T_v; these two parameters are characteristic of the experimental conditions.

The curves $log(k_v)$ versus $1/T_v$ are plotted in order to calculate the intercept and slope of this equation:

$$\log(k_v) = \log(A_{inv}) - E_{inv}/2.3RT_v \tag{5}$$

which finally results in the values of the invariant activation energy and the pre-exponential factor of the evaluated sample.

The probabilities associated with the 18 degradation functions proposed in the literature are presented in Table 2. The degradations are complex phenomena and must be represented by a set of functions instead of a single one.

Results and Discussion

The thermograms of PA6/LLDPE/SEBS-g-DEM are presented in Figure 1 for three heating rates under nitrogen atmosphere. Thermal decomposition proceeded in a single step; however, for the higher heating rate, a slight change in the slope as the sample heats up can be seen. The main decomposition step takes place in a broad temperature range (680-780 K). Moreover, the TGA thermograms of PA6/LLDPE/SEBS-g-DEM shift towards the right as the heating rate increases in the samples. No significant difference could be noticed between the thermograms with and without the interfacial agent.

DTG curves of PA6/LLDPE/SEBS-g-DEM are shown in Figure 2. Degradation rates are being shifted to higher temperatures due to the use of higher heating rates which promote a difference in the temperature profile in the sample. As the heating rate increases, there are some differences in the occurrence of the degradation reaction mechanisms. For instance, the DTG peak shifts towards the right and decrease its degradation rate as the heating rate increases (Figure 2(a)). On the other hand, PA6/LLDPE DTG curves (Figure 2(b)) do not exhibit a remarkable change on the degradation rate, possibly due to the fact that there is no interfacial area enough to reach

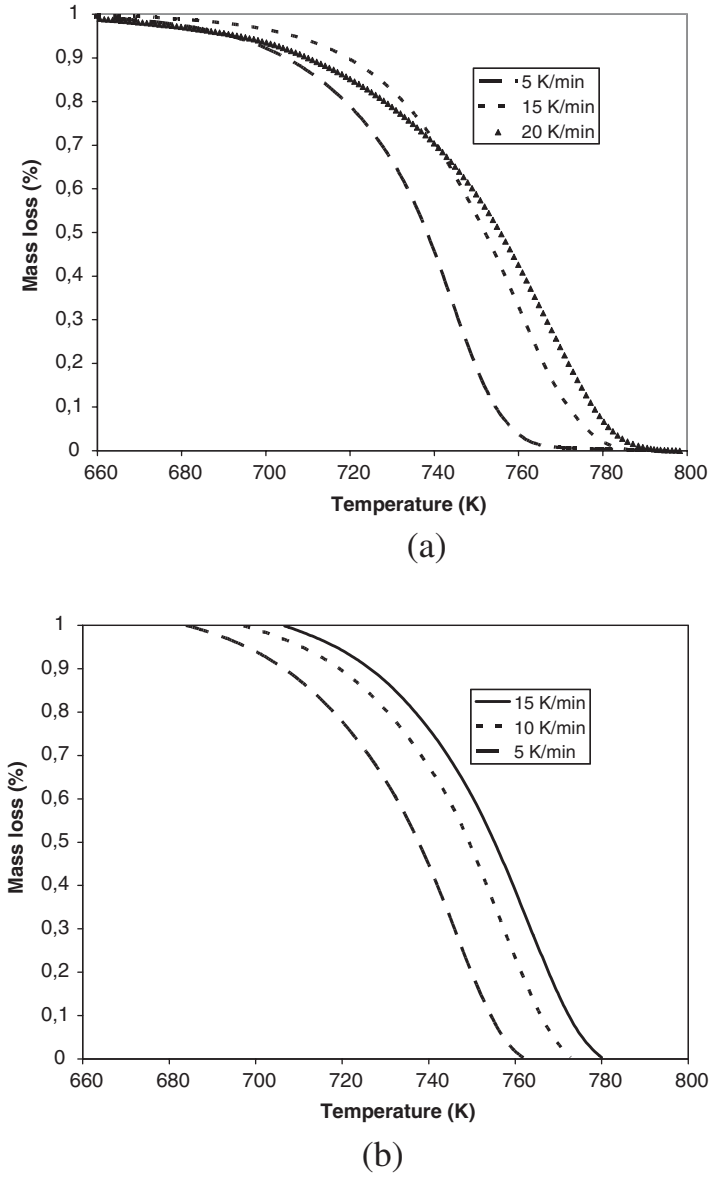

Figure 1.
(a) PA6/LLDPE/SEBS-g-DEM and (b) PA6/LLDPE thermograms.

an activation of different decomposition models.

This phenomenon is in agreement with those reported in the literature[12] on the basis of using several heating rates with the purpose of calculating the thermal kinetic parameters.

The IKP method uses the compensation effect in order to determine the values that would serve us to calculate the invariant parameters independent of the heating rate employed. Figure 3 illustrates the linear relationship found between $log(A_j)$ and E_j for PA6/LLDPE/SEBS-g-DEM blend at

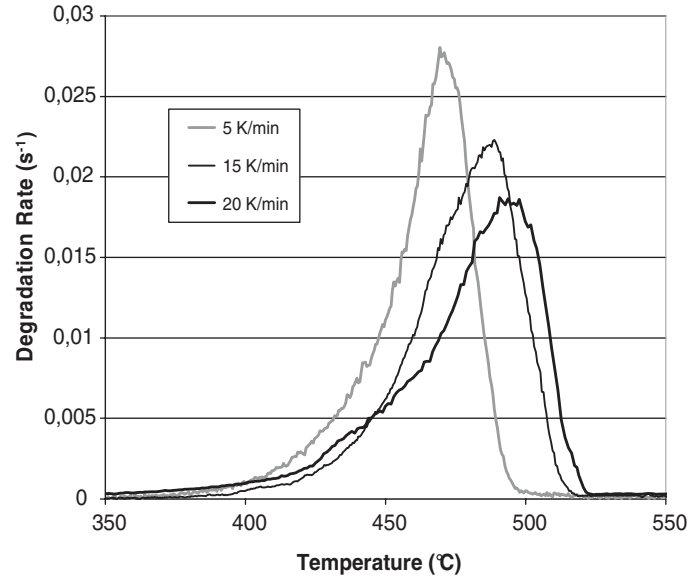

(a)

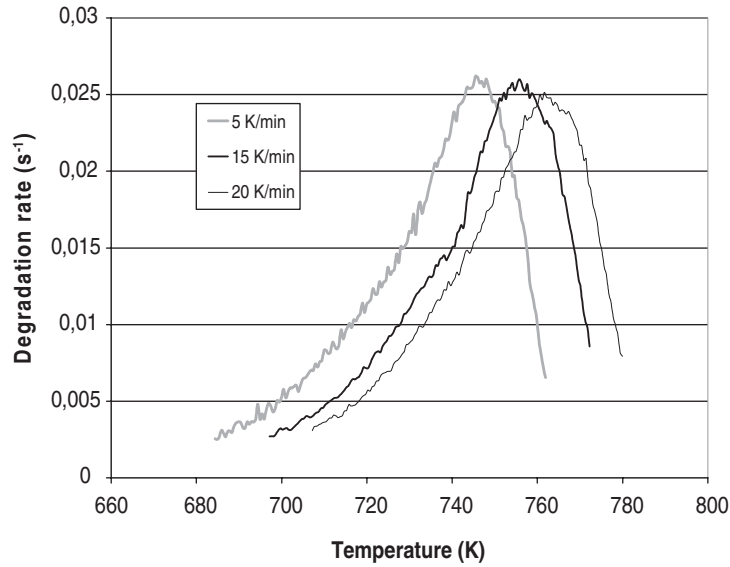

(b)

Figure 2.
DTG curves of (a) PA6/LLDPE/SEBS-g-DEM and (b) PA6/LLDPE.

several heating rates. A similar trend is observed for PA6/LLDPE blend.

Once the straight line is obtained from the apparent kinetic parameters determined through the Coats-Redfern method, the values B_v and l_v are then calculated in order to plot a new straight line whose slope and intercept correspond to the invariant activation energy and pre-exponential factor, respectively.

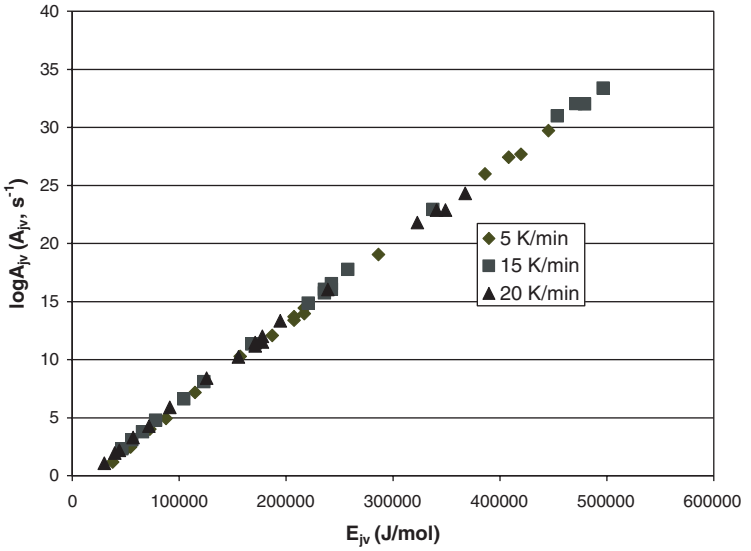

Figure 3.
Compensation effect observed in PA6/LLDPE/SEBS-g-DEM.

The invariant kinetic parameters obtained are depicted in Table 3. These results show that the addition of the interfacial agent in the PA6/LLDPE blend improves the thermal stability of the material.

The calculated invariant activation energy for the PA6/LLDPE/SEBS-g-DEM was 540 KJ/mol, which shows an increase of nearly 100% when compared to that of the PA6/LLDPE blend. This could be due to the better phase dispersion achieved when the SEBS-g-DEM is added to the blend, which is somehow improving the thermal stability of the material. Additionally, the IKP method allowed determining the probabilities of several degradation mechanisms to occur. The kinetic models assumed in the thermal decomposition are shown in Table 2.

Degradation profiles are governed by a combination of nucleation and phase boundary reactions in both of the studied blends. The probabilities of phase boundary reaction and nucleation mechanisms (Figure 4 and 5) were raised by 26%, accounting for an increase of the surface area between PA6 and LLDPE on the samples, evidencing that SEBS-g-DEM could effectively be acting as a compatibilizing agent in this blend, supporting the increase of the Ea. The Molau test also evidenced this phenomenon. Differences on material reactivities cause the blend to exhibit a thermal resistance.[13] Nucleation and nucleus growing reaction mechanisms were the most probable to take place in both samples, with and without SEBS-g-DEM.

Table 3.
Invariant kinetic parameters obtained by the IKP method.

Sample	E_{inv} (KJ/mol)	log A_{inv}
PA6/LLDPE	283	19.03
PA6/LLDPE/SEBS-g-DEM	519	35.15

On the other hand, Figure 6 presents the dependence of the kinetic functions taking place in the degradation with the degree of conversion achieved by the material. The equation plotted in Figure 6 is given by:

$$f(\alpha) = \sum_{j=1to18} (\%) f_j(\alpha) \qquad (6)$$

The continuous line represents the behavior of the PA6/LLDPE, while the

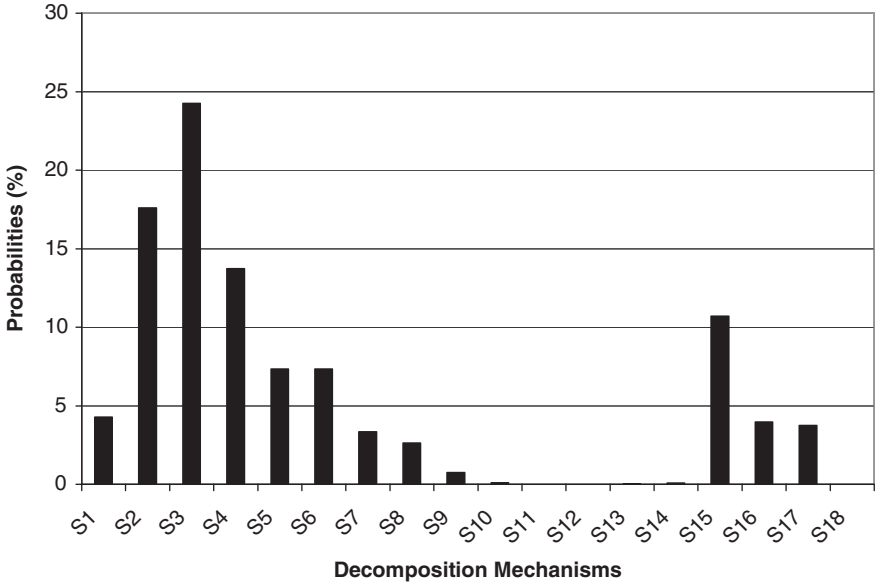

Figure 4.
Probability distribution of the 18 kinetic models used in the IKP method for the PA6/LLDPE blend.

dotted curve belongs to the PA6/LLDPE/SEBS-g-DEM. The influence of the addition of SEBS-g-DEM turns significant at early degradation stages when it starts decomposing in its surface. However, this influence decreases as the degree of conversion increases. On the other hand, for the PA6/LLDPE blends, the curve stays flat indicating that there is not a significant dependence of those kinetic models

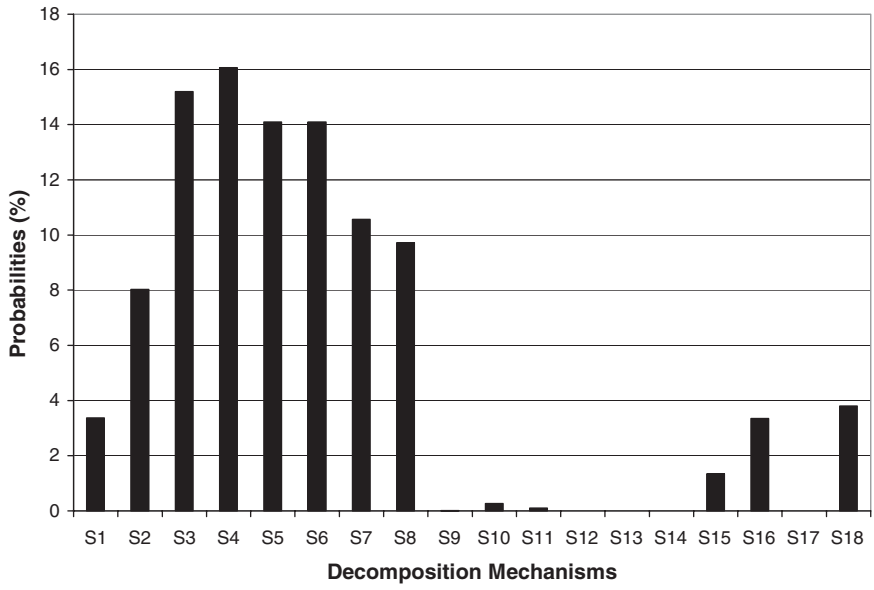

Figure 5.
Probability distribution of the 18 kinetic models used in the IKP method for the PA6/LLDPE/SEBS-g-DEM blend.

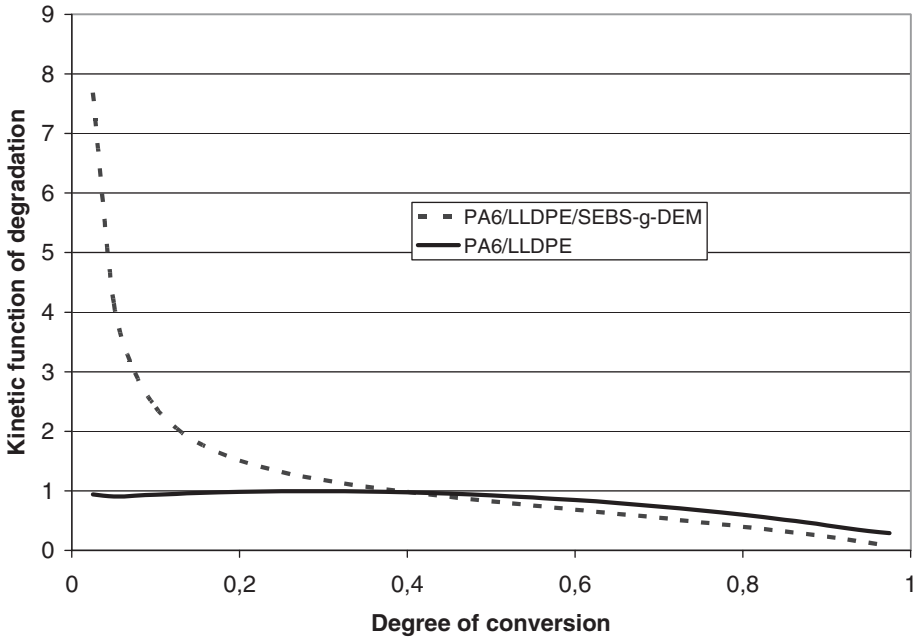

Figure 6.
Dependence of the $f(\alpha)$ with the degree of conversion (α).

occurring with the degree of conversion. Still, at lower conversion degrees, the PA6/LLDPE/SEBS-g-DEM exhibits higher function values, but when the conversion degree rises ($\alpha > 0.4$), the function values of the PA6/LLDPE/SEBS-g-DEM decreases even to lower values than those of the PA6/LLDPE, which is attributed to a protective barrier[14] due to the better phase dispersion achieved by the interfacial agent. This statement is confirmed by scanning electron microscopy (SEM). SEM micrographs are shown in Figure 7.

The degradation rates V versus α and T:

$$V = A_{inv} \times \exp(-E_{inv}/RT) \times \sum_{j=1to18} (\%) f_j(\alpha) \quad (7)$$

are plotted in Figure 8 and 9 for PA6/LLDPE and PA6/LLDPE/SEBS-g-DEM

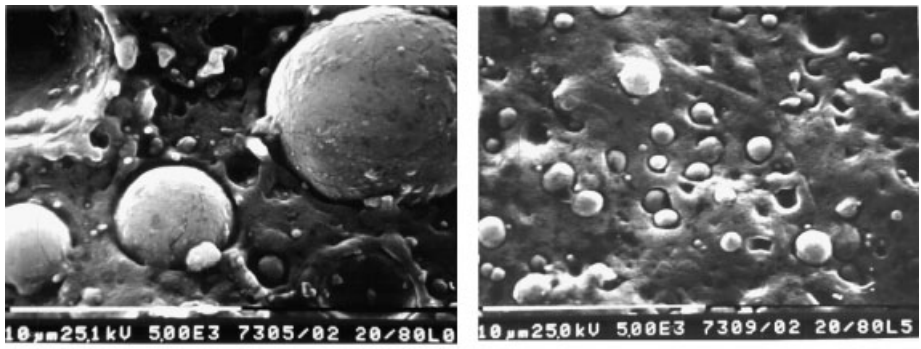

Figure 7.
SEM micrographs of (a) PA6/LLDPE and (b) PA6/LLDPE/SEBS-g-DEM.

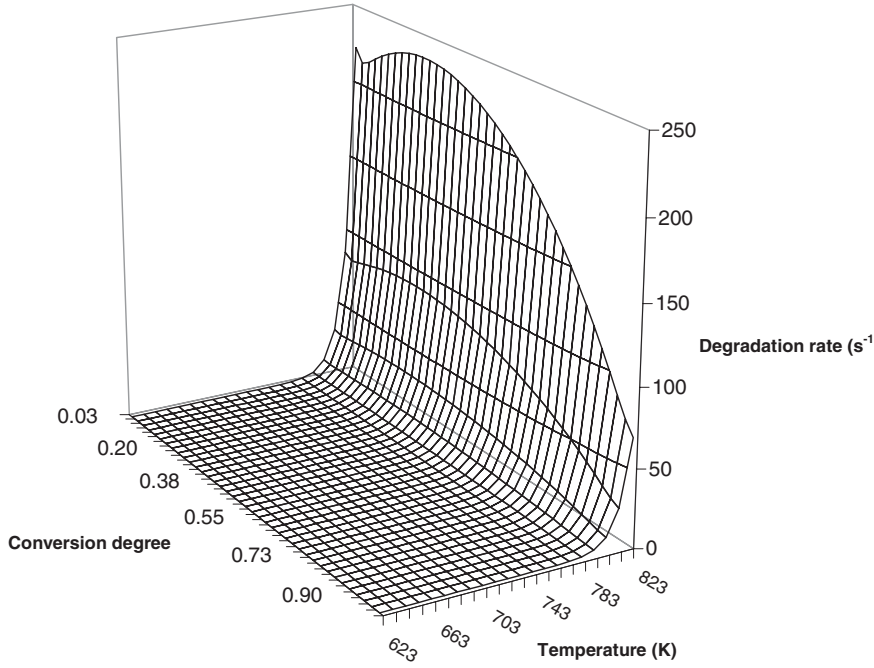

Figure 8.
Degradation rate of PA6/LLDPE versus conversion degree and temperature.

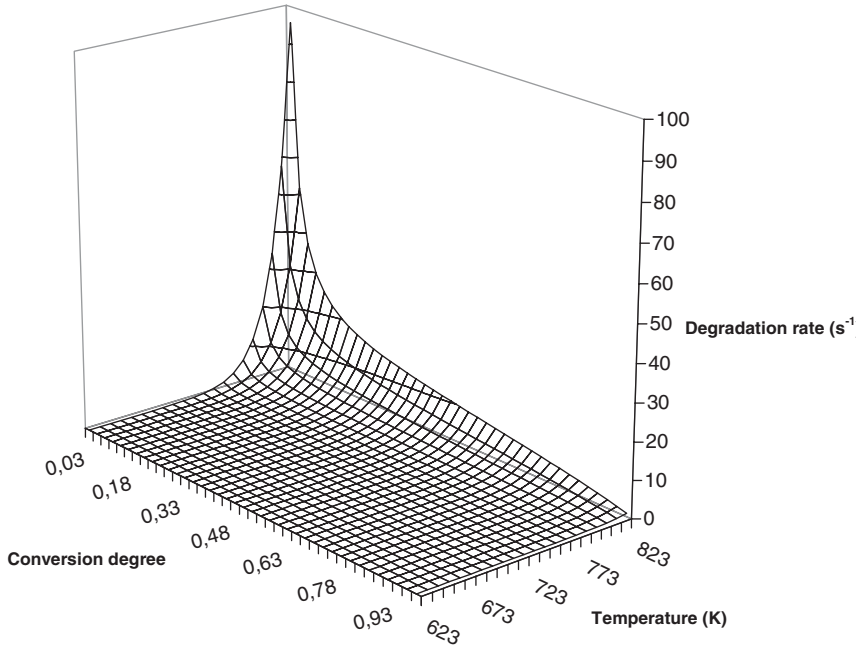

Figure 9.
Degradation rate of PA6/LLDPE/SEBS-g-DEM versus conversion degree and temperature.

samples, respectively. The 3D plots show that the blend without the interfacial agent decomposes faster at higher temperatures and at any given conversion degree than the PA6/LLDPE/SEBS-g-DEM blend. Degradation rates are lower in the blend with the interfacial agent, evidencing that its inclusion enhances the thermal stability of the blend.

Conclusions

The thermogravimetric analysis carried out in these samples showed that when the SEBS-g-DEM is added to the PA6/LLDPE there is an actual enhancement of the thermal stability due to the increase in the interfacial area within the blend. The IKP method proved to be a qualitative technique evidencing the type of degradation mechanisms taking place in the material vicinity. Nucleation and phase boundary reactions are the kinetic models on the thermal decomposition more likely of occurring. Statistical calculations along with the Molau test evidenced that the inclusion of SEBS-g-DEM in the PA6/LLDPE increases the thermal stability.

Appendix[15]

The degradation is modeled by computing the probabilities associated with the 18 degradation functions showed in Table 2. Degradation of a polymer material often cannot be represented with a single degradation function. The kinetic functions $f_j(\alpha)$ may then be discriminated using the $\log A_{inv}$ and E_{inv} values obtained. Having n of the i^{th} of the experimental values of $(\mathrm{d}\alpha/\mathrm{d}T)_{\text{iv}}$, the residual sum of squares for each $f_j(\alpha)$ and for each heating rate β_v may be computed as:

$$(n-1)S_{jv}^2 = \sum_{i=1}^{i=n}\left|\left(\frac{d\alpha}{dT}\right)_{iv} - \frac{A_{inv}}{\beta_v}\exp\left(-\frac{E_{inv}}{RT_{iv}}\right)f_j(\alpha_{iv})\right|^2 \quad \text{(A1)}$$

The most probable function is then chosen by the average minimum value of $\overline{S}_j$ defined by the relationship,

$$\overline{S}_j = \frac{1}{p}\sum_{v=1}^{v=p} S_{jv} \quad \text{(A2)}$$

where p is the number of heating rates used. The probability associated with each value $f_j(\alpha)$ can be calculated by defining the ratio,

$$F_j = \frac{\overline{S}_j^2}{\overline{S}_{\min}^2} \quad \text{(A3)}$$

where $\overline{S}_{\min}^2$ is the average minimum of residual dispersion. This ratio obeys the F distribution,

$$q(F_j) = \frac{\Gamma(v)}{\Gamma^2(v/2)}\frac{F_j^{(v/2)-1}}{(1+F_j)^v} \quad \text{(A4)}$$

where n is the number of degrees of freedom equal for every dispersion and Γ is the gamma function. It is interesting to note that the average of the residual dispersion, and not simply the residual dispersion, was chosen to define the ratio F_{j} because the average $\overline{S}_j^2$ is a good non-biased estimate of all S_{jv}^2 values and gives a better statistic representation of the process.

The probabilities of the jth function are computed on the assumption that the experimental data with L kinetic functions are described by a complete and independent system of events:

$$\sum_{j=1}^{j=L} P_j = 1 \quad \text{(A5)}$$

Therefore we obtain:

$$P_j = \frac{q(F_j)}{\sum_{j=1}^{j=L} q(F_j)} \quad \text{(A6)}$$

[1] C. Albano, J. Trujillo, A. Caballero, O. Brito, *Polymer Bulletin* **2001**, *45*(6), 531.
[2] C. J. R. Verbeek, *Material Letters* **2002**, *52*, 453.
[3] S. Bhadrakumari, P. Predeep, *Supercond. Sci. Technol.* **2006**, *19*, 808.
[4] J. Reyes, C. Albano, M. Claro, D. Moronta, *Radiation Physics and Chemistry* **2003**, *63*, 435.
[5] C. Rosales, H. Rojas, R. Perera, A. Sánchez, *J.M.S.-Pure and Applied Chemistry* **2000**, *A37*(10), 1227.

[6] S. Bourbigot, R. Delobel, M. Le Bras, D. J. Normand, *Chim. Phys.* **1993**, *90*, 1909.
[7] G. E. Molau, *J Polym. Sci.* **1965**, *3*(4), 1267.
[8] A. J. Lesnikovich, S. V. Levchik, *J. Therm. Anal.* **1983**, *27*, 83.
[9] A. J. Lesnikovich, S. V. Levchik, *J. Therm. Anal.* **1985**, *30*, 667.
[10] S. V. Levchik, G. F. Levchik, A. J. Lesnikovich, *Thermochim Acta* **1985**, *77*, 157.
[11] A. W. Coats, J. P. Redfern, *Nature* **1964**, *201*, 68.
[12] R. Serra, J. Sempere, R. Nomen, *Thermochim Acta* **1998**, *316*, 37.
[13] V. V. Boldyrev, M. Bulens, B. Delmon, The control of the reactivity of solids. Studies in Surface Science and Catalysis 2. Elsevier Scientific Publishing Company **1979**.
[14] F. Dabrowsky, S. Bourbigot, R. Delobel, M. Le Bras, *European Polymer Journal* **2000**, *36*, 273.
[15] S. Bourbigot, X. Flambard, S. Duquesne, *Polymer International* **2001**, *50*, 157.

